WE-NEED

WatEr NEEDs, availability, quality and sustainability

Deliverable Number:	D2.3
Work package number:	WP2
Deliverable title	REPORT ON PROBABILISTIC TIME RELATED PROTECTION ZONES OF THE TWO FIELD SITES
Type	Report
Dissemination Level	Public
Lead participant	UPC
Contributing scientists and other personnel	Daniel Fernàndez-Garcia, Guillem Sole-Mari, Emanuela Bianchi Janetti, Martina Siena, Ceriotti Giulia, Dell'Oca Aronne, Alberto Guadagnini, Giovanni M Porta, Monica Riva
Scheduled delivery date	20/07/2019
Actual / forecast delivery date	22/07/2019

Deliverable summary

The delineation of protection zones for wells and springs is of utmost environmental and economical relevance. We present the methodology and the results associated with the delineation of the probabilistic time-related protection zones of the two field sites: Cremona and Bologna. For the Cremona site, we identify the probabilistic recharge zones (over a total period of 5 years) associated with the main natural springs in the study area. For the Bologna site, we study the temporal evolution (over a total period of 50 years) of the probabilistic capture zones associated with the main well fields for urban supply.

D2.3
Report on probabilistic time related protection zones of the two field sites

Contents

1. Introduction

In the context of the development of new strategies for groundwater well and spring protection, it is important to define dynamic protection zones with temporal criteria, i.e., referring to the time taken by any pollutant to reach a point of interest (well/spring). Early models which have been developed to delineate protection areas and time-related capture zones are based on the assumption that the aquifer can be modelled as a homogeneous and isotropic porous medium (e.g. Bear and Jacobs, 1965; Javandel and Tsang 1986; Lerner, 1992, Kinzelbach et al. 1992; Faybishenko et al. 1995; Bakker and Strack, 1996; Schafer 1996 and Bair and Lahm 1996). The determination of protection zones in heterogeneous formations may lead to designation of protection areas of dubious reliability due to the lack of adequate site-specific values of hydraulic parameters. In these instances, a probabilistic approach can be used to estimate time-related protection zones that account for the uncertainty in the knowledge of the conceptual model to be adopted, as well as in its parameters and source terms. Franzetti and Guadagnini (1996) and Riva et al (1999) introduced the concept of time-related probabilistic well catchment and well protection zones. Riva et al (2006) analyzed the probabilistic nature of well capture zones within the well field located at the "Lauswiesen" experimental site.

In our work, we quantify the impact of (*i*) model uncertainty and (*ii*) parameters' uncertainty on the shape and the extension of well capture zones and spring recharge zones at the two field sites. In particular, for the Bologna site, the temporal evolution (over a total period of 50 years) of the probabilistic capture zones associated with the main well fields for urban supply (Tiro a Segno, San Vitale, Borgo Panigale, Fossolo and NE Bologna) is determined. An advective particle tracking method based on the interpolation of the velocity field obtained in each Monte Carlo (MC) realization generated with T-PROGS (see Deliverable D1.4b) is applied. The three-dimensional probabilistic capture zone associated with each well field of interest for a given time, t, and probability, P, is delineated.

For the pilot site of Cremona, advective transport simulations are performed via particle tracking by using the flow fields obtained from the various conceptual models previously calibrated in Deliverables D1.4b and D2.2. For these models, we identify the recharge zones associated with the main springs in the area. Probabilistic recharge zones are obtained by considering the uncertainty associated with the conductivity fields and the conceptual models considered.

1.1 Particle tracking method

We simulate solute transport via a forward-in-time advection technique, which allows us to detect the origin of the water reaching the extraction wells and to evaluate the associated travel time distributions.

Pollock's method in d dimensions (Pollock, 1988; 1994) defines the particle velocity as the d-linear interpolation of the interface velocities at any point $\mathbf{X} \in \Omega$, where Ω is a flow cell:

$$\mathbf{V} = \mathbf{v}(\mathbf{X} \in \Omega) = \left(\mathbf{1} - \hat{\mathbf{X}}\right) \odot \mathbf{v}_\Omega^- + \hat{\mathbf{X}} \odot \mathbf{v}_\Omega^+ \tag{1.1}$$

Here $\mathbf{X}$ is the particle position, $\mathbf{V}$ is the particle velocity, $\hat{\mathbf{X}} = (\mathbf{X} - \mathbf{x}_\Omega^-) \oslash (\mathbf{x}_\Omega^+ - \mathbf{x}_\Omega^-)$, $\mathbf{1}$ is a $d \times 1$ vector of ones, operators "$\odot$" and "$\oslash$" stand for the elementwise (or Hadamard) product and division, respectively, $\mathbf{x}_\Omega^-$ and $\mathbf{x}_\Omega^+$ are 3-element vectors containing the lower and upper cell interface location for each direction, and $\mathbf{v}_\Omega^-$ and $\mathbf{v}_\Omega^+$ are also 3-element vectors containing the corresponding cross-interface flow velocities (obtained in the numerical solution of the flow problem). By definition:

$$\frac{\partial \hat{\mathbf{X}}}{\partial t} = \frac{\partial \hat{\mathbf{X}}}{\partial \mathbf{X}^{\mathrm{T}}} \frac{\partial \mathbf{X}}{\partial t} = \mathbf{V}(\mathbf{X}) \oslash \Delta\mathbf{x}_\Omega = \left(\mathbf{v}_\Omega^- + \Delta\mathbf{v}_\Omega \hat{\mathbf{X}}\right) \oslash \Delta\mathbf{x}_\Omega \tag{1.2}$$

where $\Delta\mathbf{x}_\Omega = \mathbf{x}_\Omega^+ - \mathbf{x}_\Omega^-$ and $\Delta\mathbf{v}_\Omega = \mathbf{v}_\Omega^+ - \mathbf{v}_\Omega^-$. Integrating expression (1.2), given the initial velocity $\mathbf{V}(t)$, we can determine the possible lapses of time in which the particle would reach either end of the cell:

$$\Delta\mathbf{t}^+ = (\Delta\mathbf{x}_\Omega \oslash \Delta\mathbf{v}_\Omega) \ln(\mathbf{v}_\Omega^+ \oslash \mathbf{V}(t)), \qquad \Delta\mathbf{t}^- = (\Delta\mathbf{x}_\Omega \oslash \Delta\mathbf{v}_\Omega) \ln(\mathbf{v}_\Omega^- \oslash \mathbf{V}(t)) \tag{1.3}$$

In three dimensions, this gives six possible solutions, among which we choose the actual Δt as the minimum positive entry in $\Delta\mathbf{t}^+$ or $\Delta\mathbf{t}^-$; then the position of the particle at the end of the time step is:

$$\mathbf{X}(t + \Delta t) = (\Delta\mathbf{x}_\Omega \oslash \Delta\mathbf{v}_\Omega) \odot (\mathbf{V}(t) \odot \exp(\Delta t\, \Delta\mathbf{v}_\Omega \oslash \Delta\mathbf{x}_\Omega) - \mathbf{v}_\Omega^-) \tag{1.4}$$

The combined reiterated computation of expressions (1.3) and (1.4) allows to track the path of a particle of fluid in time.

2. Cremona site

We evaluate the time-related recharge zones for the same set of springs considered in the application of the Groundwater Probabilistic Risk Model (GPRM) described in Deliverable D5.2. Particle tracking simulations are performed by relying on the two conceptual models characterized by the smallest values of model discrimination criteria (*NLL* and *KIC* indices) as detailed in Table 2.2 of Deliverable D1.4b: *Composite Medium* (*CM*) and *Overlapping continua* (*OC_A*). Section 2.1 summarizes key results of flow model calibration. Section 2.2 describes the probabilistic approach here employed to account for the uncertainty in the conductivity field and in the conceptual model. Key results of the evaluation of probabilistic recharge zones are embedded in Section 2.3.

2.1 Flow model output

In this Section we report updated results of model calibration developed on the basis of the analysis reported in Deliverables D1.4a and D1.4b. According to the results of the Global Sensitivity Analysis (in Deliverable D1.4a), we calibrate parameters k_1, k_3 and k_5 for the *CM* model and k_3, k_5 for the *OC_A* model. For each conceptual model, insensitive parameters are fixed to values consistent with the geological features of the corresponding classes, as reported in Table 2.5 of Deliverable D1.4a. We then focus on the calibration of the spring leakage coefficient for each one of the two conceptual model analyzed (see Deliverable D1.4b).

Here we update the results of Deliverable D1.4b by considering yearly-averaged hydraulic heads collected at 35 out of 39 measurement points (see Figure 2.1a). This choice relies on the fact that the four neglected measurements are located very close to the boundaries and, therefore, are more affected by the boundary conditions rather than by the heterogeneous hydraulic properties of the field. New results are embedded in this section. We refer to Section 2.2 in Deliverable D1.4b for the description of the methodology.

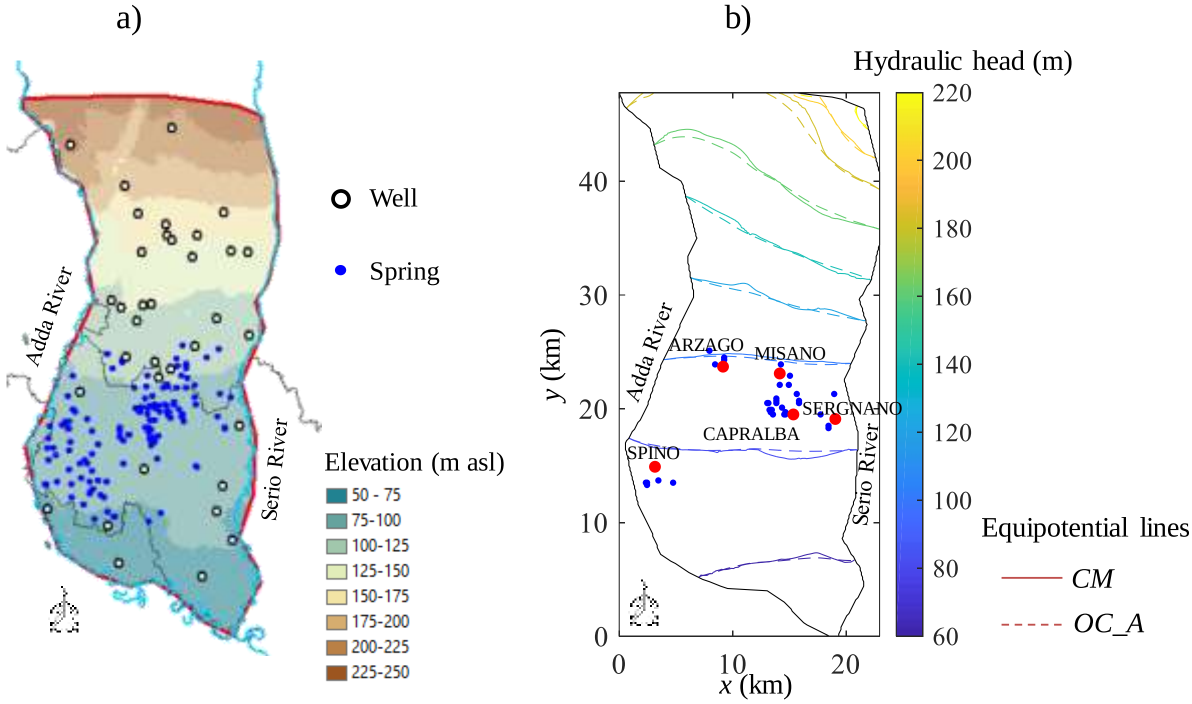

Figure 2.1 a) Location of observation wells and springs in the study area; b) Spatial variation of hydraulic heads associated with *CM* and *OC_A* calibrated models.

	CM			*OC_A*		
	k	LB	UB	*k*	LB	UB
k_1 (m/s)	4.03×10^{-5}	3.34×10^{-5}	4.87×10^{-5}	1.00×10^{-6}	-	-
k_2 (m/s)	1.00×10^{-4}	-	-	1.00×10^{-4}	-	-
k_3 (m/s)	2.15×10^{-2}	8.48×10^{-3}	5.45×10^{-2}	1.80×10^{-2}	8.45×10^{-3}	3.83×10^{-2}
k_4 (m/s)	1.00×10^{-5}	-	-	1.00×10^{-5}	-	-
k_5 (m/s)	1.21×10^{-3}	5.62×10^{-3}	2.59×10^{-2}	9.93×10^{-3}	3.13×10^{-3}	3.15×10^{-2}

Table 2.1: Parameter estimates of the two conceptual models analyzed. Lower bound (LB) and upper bound (UB) of the 95% confidence limits are also reported.

Figures 2.1 depicts the location of springs and observation wells (Fig. 2.1a) and the spatial variation of hydraulic heads associated with *CM* and *OC_A* calibrated models (Fig. 2.1b). The main flow direction is from North to South. The hydraulic gradient decreases slightly from North to South, with a mean value of approximately 3.7‰. One can note that the distribution of hydraulic heads in the calibrated models do not present significant difference between the two approaches considered. As discussed below, both calibrated models are accurate in reproducing the behavior of the main flow feature of the site (e.g., hydraulics heads) as well as the mean annual total discharge at the natural springs.

Conductivity estimates of each facies are reported in Table 2.1 for the two conceptual models. Lower (LB) and upper (UB) bounds of 95% confidence intervals, calculated according to a Maximum Likelihood methodology, are also included for all estimated parameters. The hydraulic conductivity values estimated are consistent with the geological features of the classes and are very close to those obtained in Deliverable D1.4b. For all conceptual models, the lowest value is associated with the clay, silt and fine sand materials, corresponding to Classes 1 and 2, while the largest conductivities are related to the gravel material and to the fractured conglomerate, corresponding to Classes 3 and 5.

Parameter	**Symbol**	***CM***	***OC_A***	**Unit**
Leakage coefficient	l_d	1.21×10^{-6}	1.30×10^{-6}	s^{-1}
Total spring flow rate	Q_s	14.44	14.59	m^3/s

Table 2.2. Values of calibrated leakage coefficient.

Table 2.2 reports the values of the leakage coefficient (see Deliverable D5.2) at the end of the inversion process and the predicted values of the total spring flow rate for the two conceptual models, i.e. *CM* and *OC_A*. These results are associated with the boundary condition set BC_3 (i.e. p_6 = 19.30 m^3/s and p_7 = 3.0 m), corresponding to the best optimization results for *CM* and *OC_A* (see Table 2.4 of Deliverable D1.4a). The estimated leakage coefficients are similar in the two models and allow to predict values of total spring flow rate that are close to their measured counterpart (= 14.62 m^3/s).

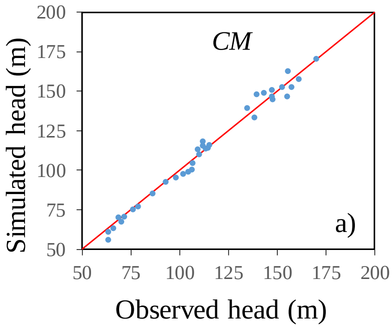

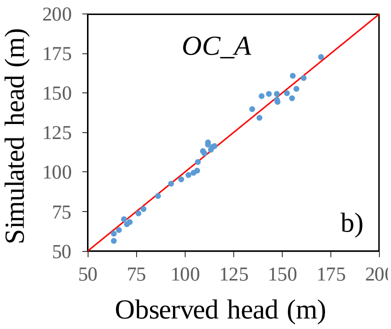

Figure 2.2. Simulated versus observed hydraulic head at the monitoring stations. Simulated heads have been obtained with the a) *CM* and b) *OC_A* approaches.

	CM	***OC_A***
J	**602**	610
σ_h^2	15.43	15.65
NLL	**195.1**	195.6
AIC	201.1	**199.6**
AICc	201.9	**200.0**
BIC	205.8	**202.7**
KIC	203.9	**198.7**

Table 2.3. Inversion statistic for the two conceptual models and model identification criteria. Minima amongst all models are in bold.

The diverse water balance terms evaluated for the two models are depicted in Figure 2.3 and they are similar with those discussed in Deliverable D2.2. All incoming terms are indicated with subscript “in” while quantities outflowing from the aquifer are indicated with subscript “out”. The conceptual model mainly affects the amount of water entering and/or leaving the aquifer through the Western and Eastern boundaries of the domain (which correspond to the flow paths of Adda and Serio rivers). All remaining terms are not significantly affected by model conceptualization.

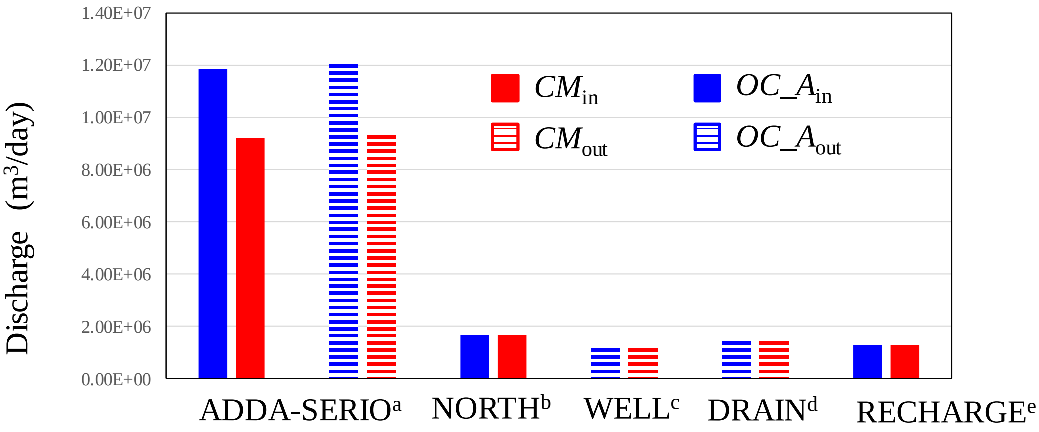

Figure 2.3. Water balance terms evaluated for *CM* and *OC_A* calibrated models. Different terms correspond to flow rates due to (a) Eastern and Western domain boundaries, (b) Northern domain boundary, (c) pumping wells, (d) natural springs and (e) recharge from infiltrations.

2.2 Probabilistic approach for the delineation of spring protection zones

As described in Section 2.1, we consider two sources of uncertainty (a) Conceptual Model Uncertainty and (b) Model parameters' uncertainty. Conceptual Model Uncertainty is included by considering two diverse reconstructions of the Cremona geological features. Uncertain parameters are N_p log-conductivity values, Y_i=logk_i, associated to the most influential geomaterials constituting the aquifer system (identified in Deliverable D1.4b), i.e. Y_i values associated with (*i*) clay (37 %), gravel (30 %) and fractured conglomerate (15 %) for *CM* rendering N_p = 3 and (*ii*) gravel and fractured conglomerate for *OC_A*, rendering N_p = 2.

For completeness, we report here the main steps of the methodology employed for the generation of log-conductivity fields (additional details can be found in Section 3.3 of Deliverable D5.2).

We denote by **Y** the vector of values of Y_i (i =1, N_p). The latter has been calibrated through a Maximum Likelihood (ML) approach (see Section 2.1) that resulted in a mean value ($\boldsymbol{\mu}$) of **Y** and in a posterior covariance matrix ($\boldsymbol{\Sigma}$). We therefore consider **Y** as an N_p-uncertain parameters' vector, characterized by a multivariate gaussian distribution with mean $\boldsymbol{\mu}$ and covariance $\boldsymbol{\Sigma}$. ML estimates ($\boldsymbol{\mu}$) of the log-transformed calibrated parameters (Y_i=logk_i) and estimation error covariance matrices ($\boldsymbol{\Sigma}$) are reported in Table 2.4.

Groundwater Model	ML estimates	Estimation error covariance matrix
CM	$\boldsymbol{\mu}=[-4.39,-1.67,-1.92]$	$\boldsymbol{\Sigma}=\begin{bmatrix} 1.62\times10^{-3} & -2.57\times10^{-3} & 4.90\times10^{-3} \\ \cdots & 3.63\times10^{-2} & -1.40\times10^{-2} \\ \cdots & \cdots & 2.65\times10^{-2} \end{bmatrix}$
OC_A	$\boldsymbol{\mu}=[-1.74,-2.00]$	$\boldsymbol{\Sigma}=\begin{bmatrix} 2.60\times10^{-2} & 2.07\times10^{-2} \\ \cdots & 6.07\times10^{-2} \end{bmatrix}$

Table 2.4. Statistical parameters of the multivariate normal distributions considered in the analysis.

We randomly extract a sample of N = 100 data from each one of the multivariate normal distributions in Table 2.4. For each point of these samples (depicted in Figure 2.4) we solve the flow model described in Deliverable D1.4a. Flow model outputs are used for the computation of flow velocities needed as inputs of the particle tracking method described in Section 1.1 and implemented as follows.

Porosity is set equal to 0.25. At $t = 0$, a particle is placed at the center of each active and non-dry cell of the domain, for a total of $\approx 10^6$ particles. Particle movement is simulated via Eq (1.4). A particle is removed from the simulation when it reaches the domain boundaries, a pumping well or a spring.

For a given realization, the three-dimensional time-dependent t_i-recharge zone of a spring is defined by the set of initial positions of all particles reaching the spring within a time smaller than or equal to t_i. We then evaluate, on the basis of N flow and transport simulations, the probability $P(\boldsymbol{x}, t_i)$ of a particle injected at a location $\boldsymbol{x}$ to reach a spring within a given time t_i.

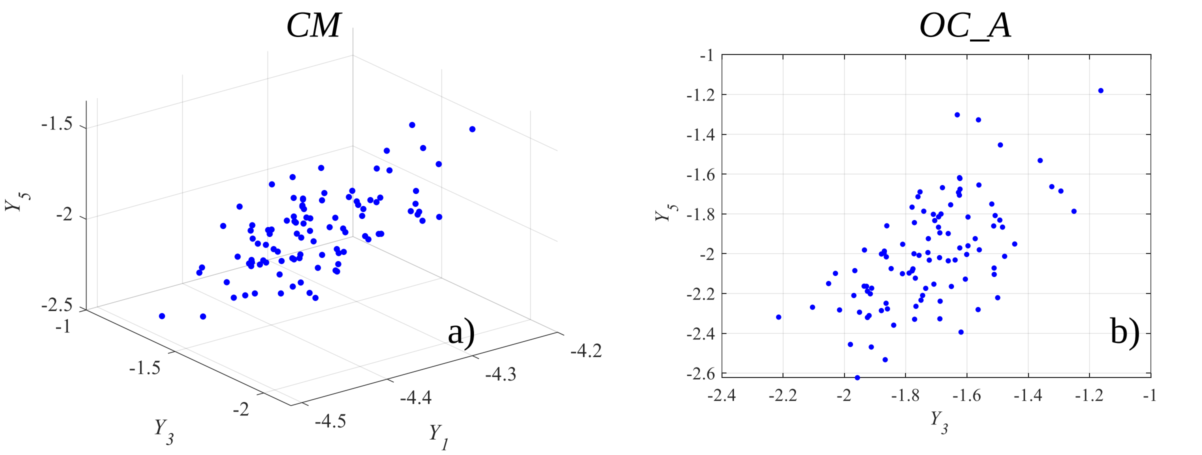

Figure 2.4 Sample of size $N = 10^2$ from the multivariate *pdfs* of the parameter estimates for a) *CM* and b) *OC_A* approaches.

2.3 Results and discussion

We focus our analysis on the set of 34 springs considered in Deliverable D5.2 for the application of the GPRM (the location of these springs is reported in Figure 2.1b and in Annex II of Deliverable D5.2). Here, as in Deliverable D5.2, we group the springs by the name of the closest well, obtaining a total of 5 groups: Arzago (BG), Misano (BG), Capralba (CR), Sergnano (CR) and Spino (CR). Figure 2.5 shows a three-dimensional representation of the recharge zones of all springs within a single realization of the *CM* model at four different times: (a) 60 days, (b) 1 years, (c) 2 years and (d) 5 years. The distribution of facies is also depicted in background. Analogous results for a single realization of the *OC_A* model are depicted in Figure 2.6. It can be noted that for both models the spring recharge zones are mainly located in the NE sector of the domain.

Figures 2.7 and 2.8 depict horizontal and vertical projections of probabilistic recharge zones computed with P = 95%, for various times and for *CM* and *OC_A* models respectively. These pictures allow to investigate the effects of different conceptual models of the aquifer heterogeneity structure on the delineation of three-dimensional time-related spring recharge zone.

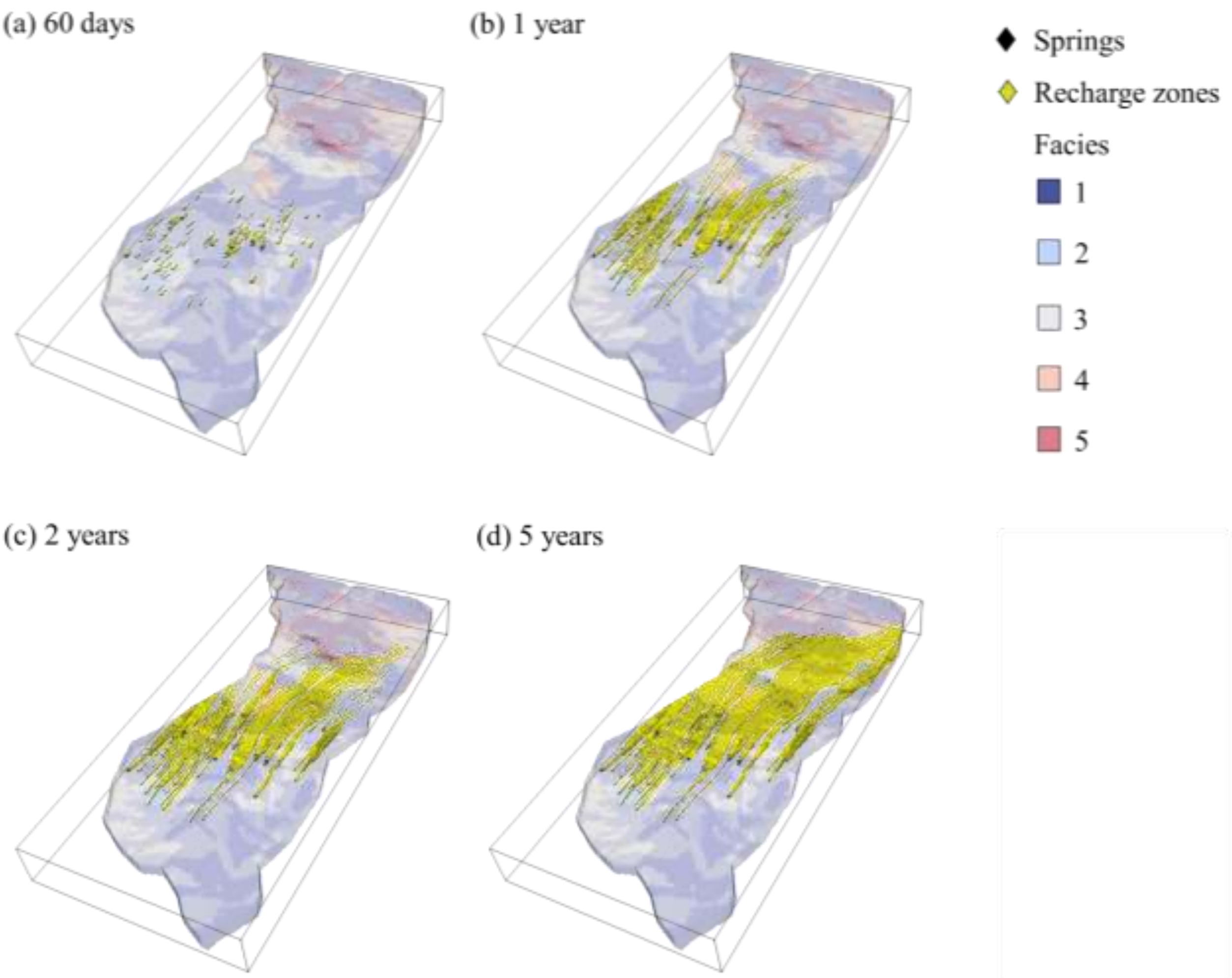

Figure 2.5. Time related recharge zones of springs evaluated within a single realization of the *CM* model for t = (a) 60 days, (b) 1 year, (c) 2 years and (d) 5 years.

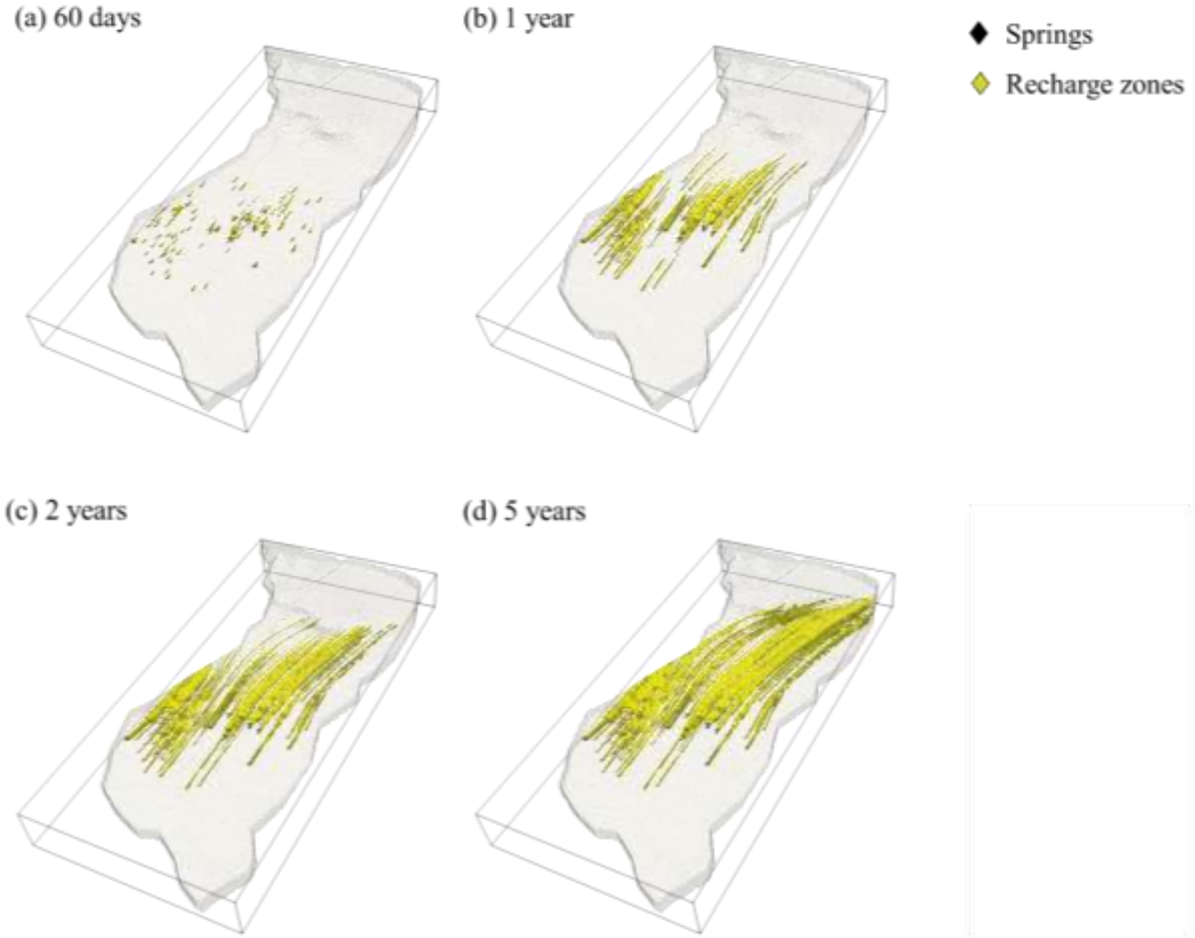

Figure 2.6. Time related recharge zones of springs evaluated within a single realization of the *OC_A* model for t = (a) 60 days, (b) 1 year, (c) 2 years and (d) 5 years.

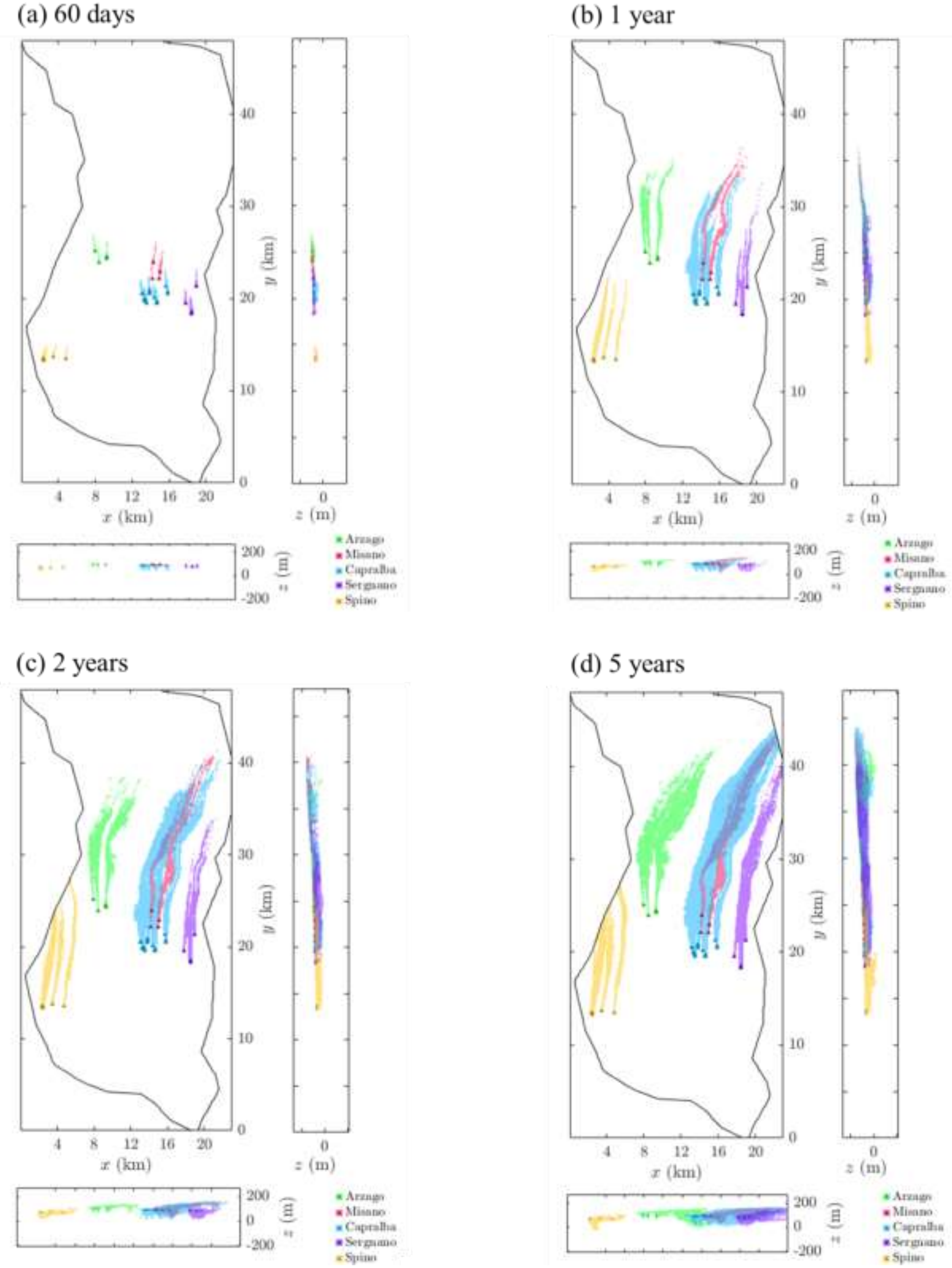

Figure 2.7. Horizontal and vertical projections of probabilistic springs recharge zones evaluated with P = 95% and at time: (a) 60 days, (b) 1 year, (c) 2 years and (d) 5 years for *CM*.

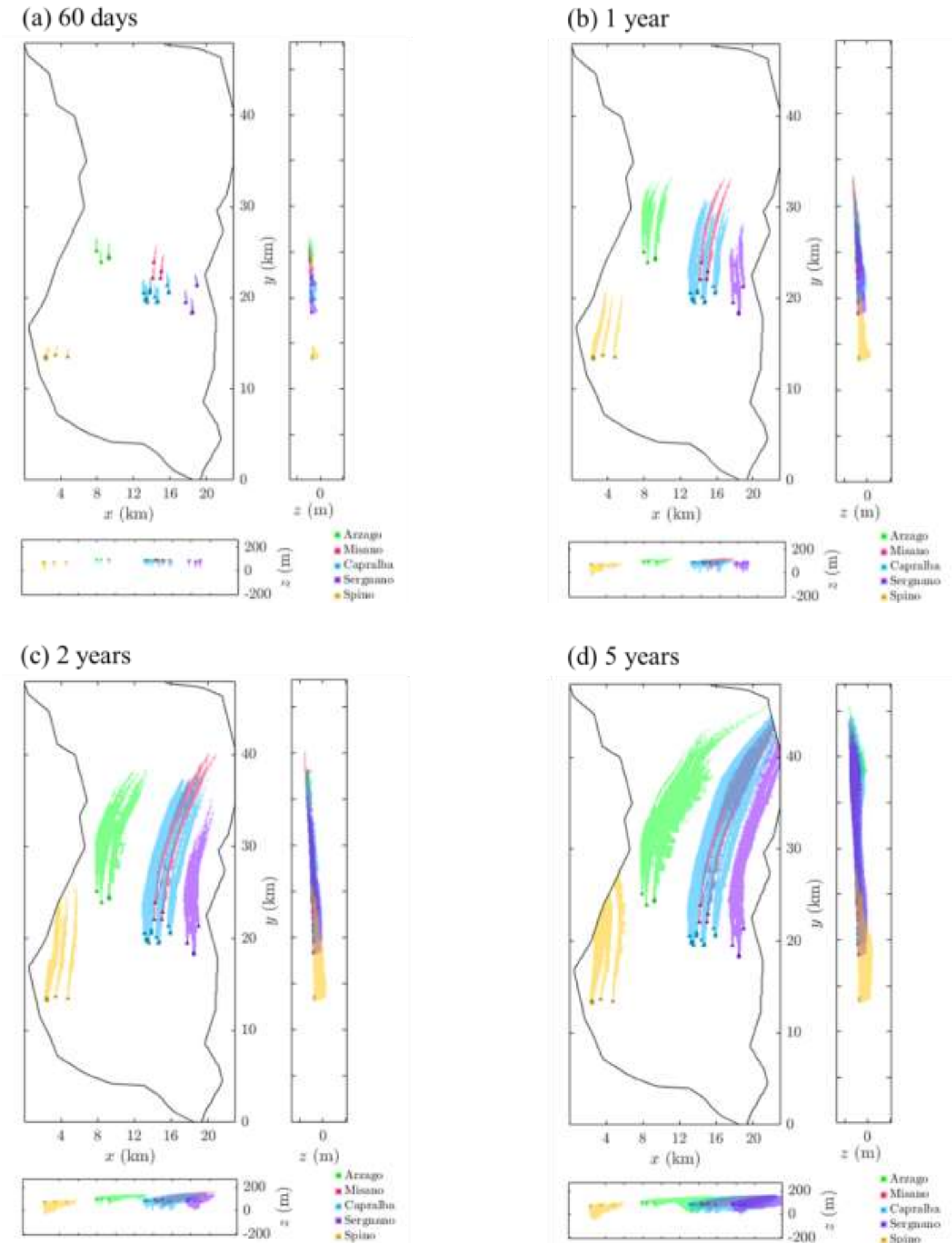

Figure 2.8. Horizontal and vertical projections of probabilistic springs recharge zones evaluated with P = 95% and at time: (a) 60 days, (b) 1 year, (c) 2 years and (d) 5 years for *OC_A*.

3. Bologna site

3.1 Flow model output

We implement the advective particle tracking described in Section 1.1 within each MC flow solution resulting from the numerical simulation of groundwater flow performed in all geological reconstructions of the Bologna field obtained with T-PROGS. Details about conceptual and numerical model have been provided in Deliverables D1.4b and D2.2. Here, to improve the accuracy of the flow solution to be used as input of the transport model, we increase the numerical grid resolution. As illustrated by Fig. 3.1a, the grid size along both horizontal axes decreases progressively from 500 m to 125 m, moving from the external boundaries to internal region where the most important well fields are located

As observed in Deliverable D2.2, a common feature of the distributions of hydraulic heads in all realizations is the cone of drawdown centered on the main well fields in the Bologna urban area, superimposed to the main natural flow (directed towards the y axis). This is also evident from Fig. 3.1b, where the aquifer' zones characterized by hydraulic heads below the threshold h = 0 are depicted.

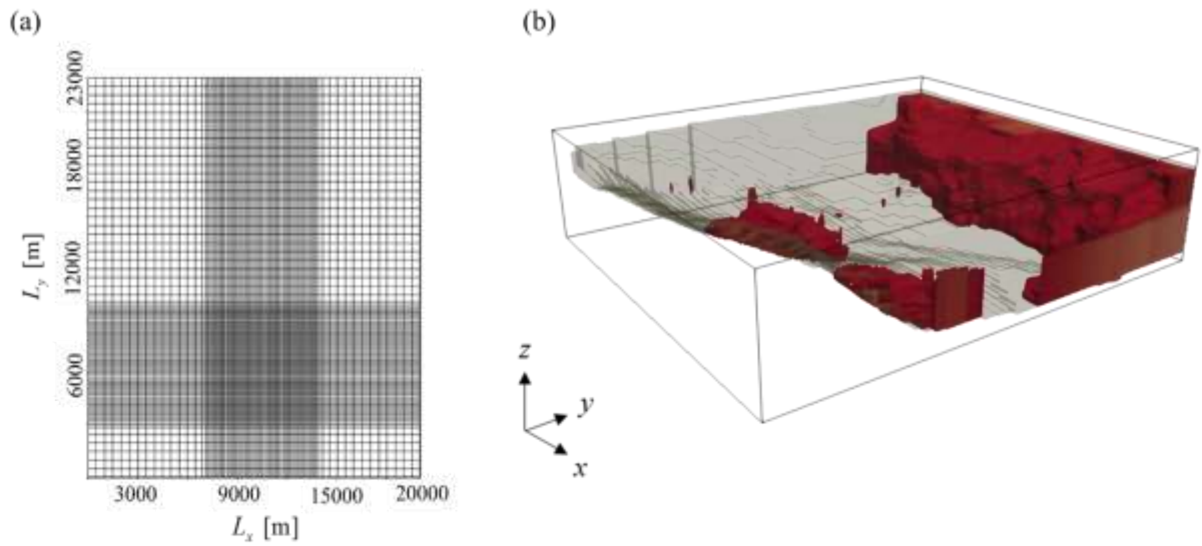

Figure 3.1. (a) Refined grid used for groundwater flow and transport simulations.
(b) Numerical flow solution in a single realization: the contour volume of hydraulic heads with values h < 0 is depicted in red.

3.2 Probabilistic approach for the delineation of well protection zones

In the Bologna case, we consider the uncertainty in the distribution of geological facies. Each one of the N = 100 equally probable realizations of random facies distributions has been calibrated on the basis of available hydraulic head observations (see Deliverable D1.4b) to determine hydraulic conductivity estimates associated to the two predominant facies (i.e., clay and gravel). The obtained flow solution is the primary input to generate the individual capture zones of each well by applying Eq. (1.4). Here, we expect a higher variability in the results with respect to the Cremona site, since, in this case, not only the hydraulic conductivities of the facies, but also the spatial distribution of facies are uncertain.

Simulations are set as follows. Numerical particles are placed inside the domain at $t = 0$ with uniform spacing of $125\ \mathrm{m} \times 125\ \mathrm{m} \times 5\ \mathrm{m}$, corresponding to the smallest flow cell size. Porosity is set equal to 0.25. The particles, transported by advection, are removed from the simulation when they reach either the domain boundaries or an extraction well. The three-dimensional time-related t_i-capture zone of a well in each realization is defined by the set of initial positions of all particles extracted by that well within a time smaller than or equal to t_i. The statistical analysis of the population of N results leads to the concept of probabilistic time-related capture zones, which can be studied with reference to the total probability, P, of capture within a given time.

3.3 Results and discussion

We focus our analysis on the 10 wells with the highest extraction rate in the region (see Deliverable D2.2 for details). In this case, we group them by well fields, when relevant, for a total of 5 differentiated groups: San Vitale, Tiro a Segno, Borgo Panigale, North-East Bologna and Fossolo. Figure 3.2 provides a three-dimensional representation of the joined capture zones of all well fields within a single MC realization computed for four different times: (a) 60 days, (b) 2 years, (c) 10 years and (d) 50 years. The distribution of facies is also depicted in background. It can be noted that the progressive enlargement of the capture zone is not homogeneous all along the well screen, being respectively lower (faster) in presence of low- (high-) conductivity regions.

Figures 3.3 and 3.4 depict horizontal and vertical projections of probabilistic time related capture zone computed with P = 95% for various times.

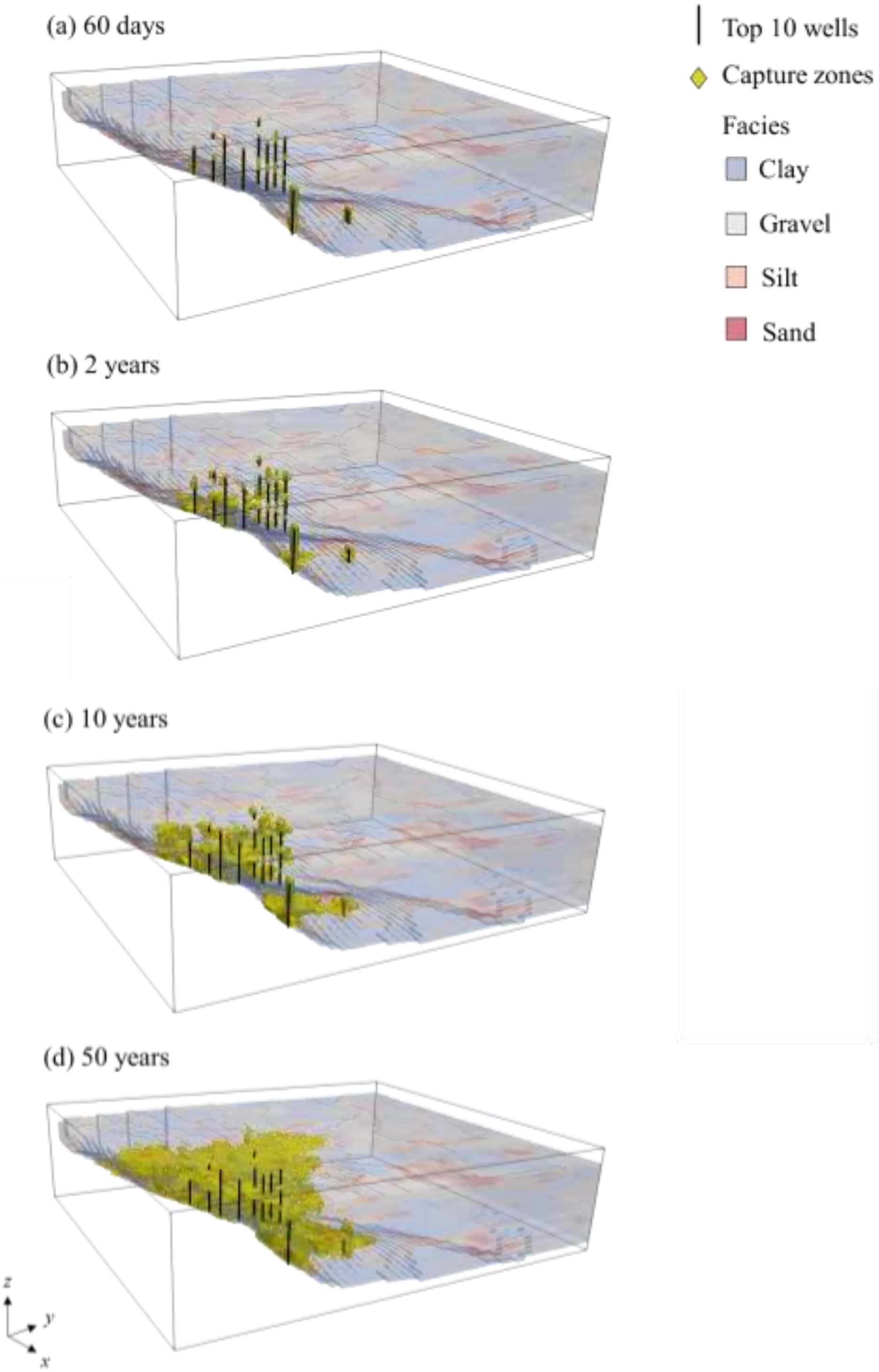

Figure 3.2. Capture zones of all the main well fields within a single realization at times (a) 60 days, (b) 2 years, (c) 10 years and (d) 50 years.

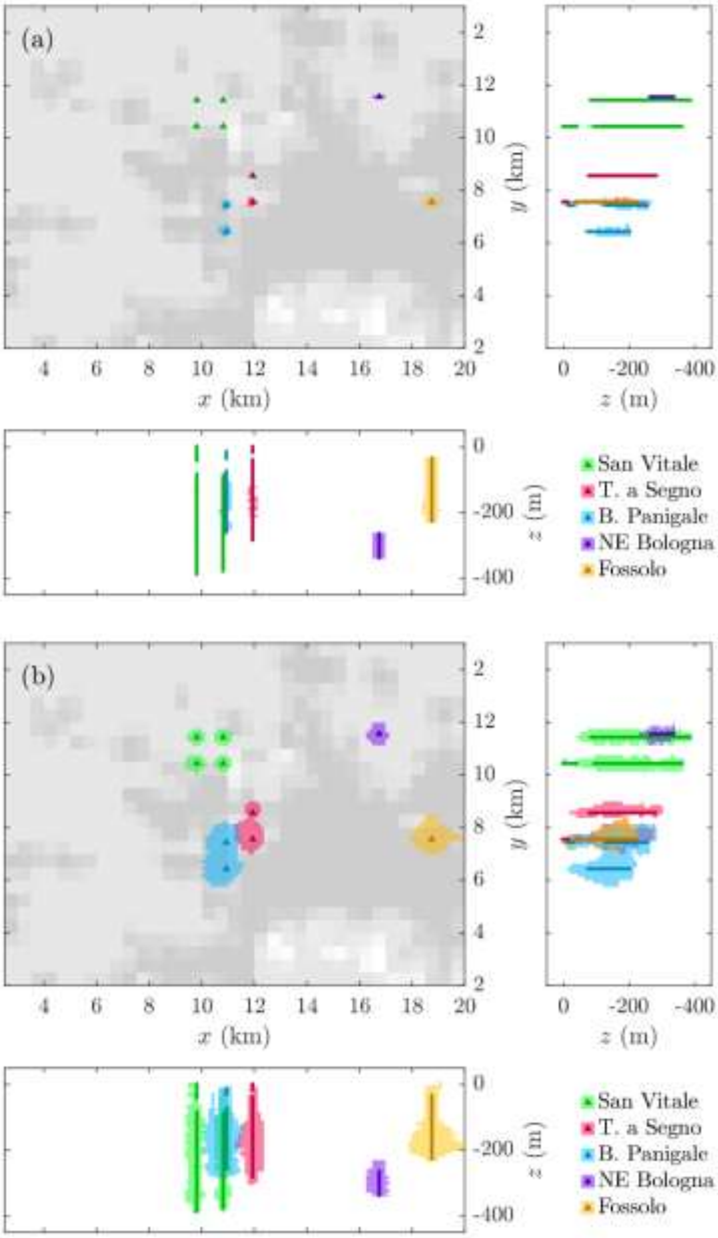

Figure 3.3. Horizontal and vertical projections of probabilistic time-related capture zones evaluated with P = 95% at t = (a) 60 days and (b) 2 years. In the horizontal projections, the urban area of Bologna is depicted, dark grey representing industrial and urban zones, mild grey representing the agricultural land, and white color representing the non-anthropized areas.

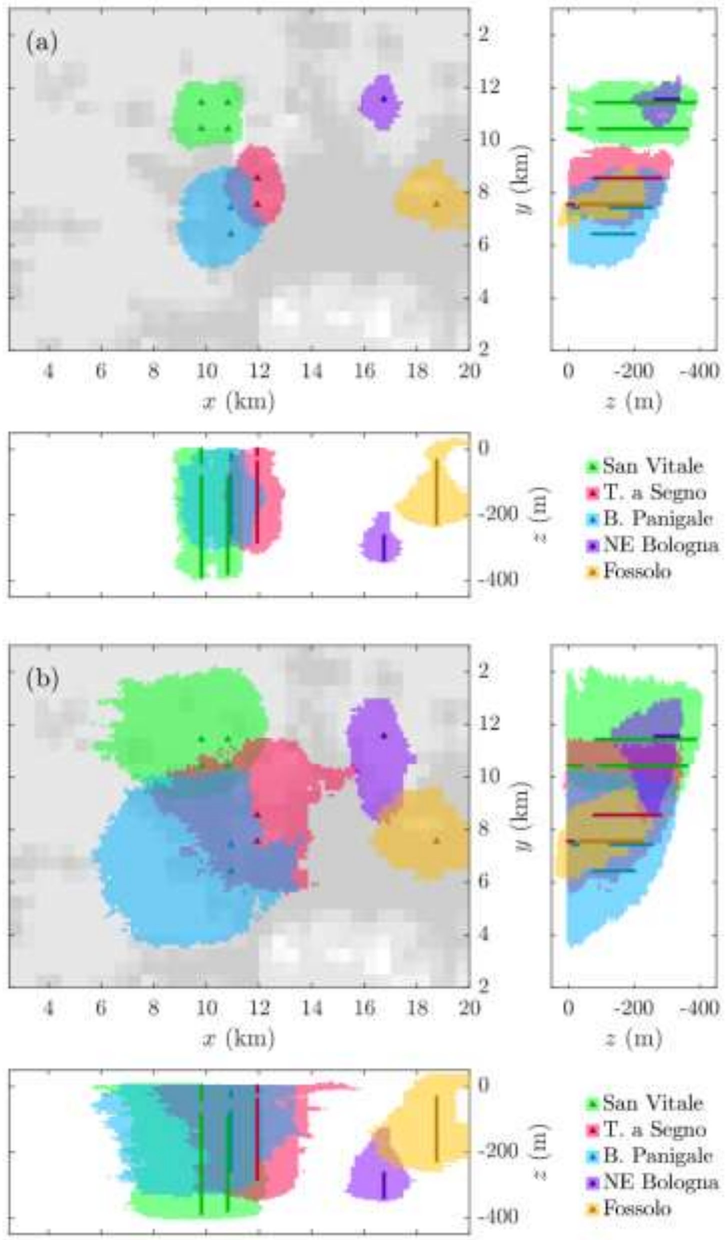

Figure 3.4. Horizontal and vertical projections of probabilistic time related capture zones evaluated with P = 95% at t = (a) 10 years and (b) 50 years. In the horizontal projections, the urban area of Bologna is depicted, dark grey representing industrial and urban zones, mild grey representing the agricultural land, and white color representing the non-anthropized areas.

4. Conclusions

We analyze the probabilistic nature of spring recharge zones and well capture zones within the Cremona and the Bologna site, respectively. The results illustrated here can be used as a first-screening tool within a risk assessment procedure. Our outcomes allow to delineate, within a stochastic framework, the three-dimensional regions that are most critical for the two sites and, therefore, the areas to which stakeholders and decision makers should devote more attention. In other words, groundwater bodies not belonging to any of the probabilistic capture or recharge zones that we evaluate with a given probability (95%) and for diverse times are very unlikely (*i*) to be extracted by any of the considered wells or (*ii*) to recharge any of the springs, within the time windows considered. The study here performed must be achieved jointly with the water authorities in order to set the probability that can be associated to an acceptable level of risk and the time of interest.

For the Bologna site, the growth of the probabilistic capture zone is very slow (indicative of high residence times), due to the high water volume capacity of the aquifer system, with a thickness of hundreds of meters. Additionally, the rather large scale of the model restricts our analysis to correspondingly large (spatial and temporal) scales of the capture zones.

According to our results, the deep well denominated as NE Bologna is well protected by surface contamination: its 95% capture zone does not reach the ground surface even after 50 years of pumping. All the remaining well-fields are characterized by capture zones that reach the ground surface within ~10 years. The Borgo Panigale well field exhibits the most extended capture zone along the horizontal directions. This behavior is mainly due to the smaller aquifer thickness at its location, as compared, e.g., to the San Vitale well field, whose capture zone is, on the other hand, more extended along the vertical direction.

For the Cremona site, the growth of the probabilistic protection zones is faster compared to the Bologna site. This result is related to the presence of a stronger hydraulic gradient from North to South which leads to larger groundwater flow velocities in the Cremona rather than in the Bologna area.

We refer to Deliverable D5.2 for a probabilistic approach for the evaluation of the risk associated with (*i*) the extraction of contaminated groundwater, when the source of contamination is located at the top of the aquifer (Bologna site) and (*ii*) the depletion of natural springs (Cremona site).

References

Bakker, M., Strack, O.D.L., 1996. Capture Zone Delineation in Two-Dimensional Groundwater Flow Models. Water Resour. Res. 32 (5), 1309-1315.

Bair, E.S., Lahm, T.D., 1996. Variation in capture-zone geometry of a partially penetrating pumping well in an unconfined aquifer. Ground Water 34 (5), 842–852.

Bear, J. Jacobs, M., 1965. On the Movement of Water Bodies Injected into Aquifers. J. Hydrol. 3, 37-57.

Deliverable D1.4a, Report on characterization of field sites, WE-NEED, 2018.

Deliverable D1.4b, Report on characterization of field sites, WE-NEED, 2018.

Deliverable D2.2, Report on groundwater flow and transport on the two field sites, WE-NEED, 2018.

Deliverable D5.2, Report on the application of the risk model to the field sites, WE-NEED, 2019.

Faybishenko, B.A., Javandel, I., Witherspoon, P.A., 1995. Hydrodynamic of the capture zone of a partially penetrating pumping well in an unconfined aquifer. Water Resour. Res. 31 (4), 859–866.

Franzetti, S., Guadagnini, A., 1996. Probabilistic estimation of well catchments in heterogeneous aquifers. J. Hydrol. 174, 149-171.

Guadagnini, A, Franzetti, S., 1999. Time-related Capture Zones for Contaminants in Randomly Heterogeneous Formations. Ground Water 37 (2), 253-260.

Guadagnini, A., Guadagnini, L., Tartakovsky, D.M., Winter, C.L., 2003. Random domain decomposition for flow in heterogeneous stratified aquifers. Stoch. Environ. Res. Risk Assess. 17, 394–407. doi:10.1007/s00477-003-0157-1.

Guadagnini, L., Guadagnini, A., Tartakovsky, D.M., 2004. Probabilistic Reconstruction of geologic facies. J. Hydrol. 294, 57-67.

Javandel, I., Tsang, C.-F., 1986. Capture-Zone Type Curves: A Tool for Aquifer Cleanup. Ground Water 24, 616-625.

Kinzelbach, W., Marburger, M., Chiang, W.-H., 1992. Determination of groundwater catchment areas in two and three spatial dimensions. J. Hydrol. 134, 221-246.

Lerner, D.N., 1992. Well Catchments and Time-of-Travel Zones in Aquifers with Recharge. Water Resour. Res. 28, 2621-2628.

Pollock, D.W. (1988). Semianalytical computation of pathlines for finite-difference models. Ground Water 26, 743.

Pollock, D.W. (1994). User’s guide for MODPATH/MODPATHPLOT, Version 3: A particle tracking post-processing package for MODFLOW. The U.S. Geological Survey finite-difference groundwater flow model. U.S. Geological Survey Open-File Report 94–464, Reston,VA: U.S. Geological Survey

Riva, M, Guadagnini, A, Ballio, F., 1999. Time related capture zones for radial flow in two-dimensional randomly heterogeneous media. Stoch. Environ. Res. Risk Assess. 13 (3), 217-230.

Riva, M., Guadagnini, L., Guadagnini, A., Ptak, T., Martac, E., 2006. Probabilistic study of well capture zones distribution at the Lauswiesen field site. J. Contam. Hydrol. 88, 92–118.

Schafer, D.C., 1996. Determining 3D Capture Zones in Homogeneous, Anisotropic Aquifers. Ground Water 34 (4) 628-639.